# CHAPTER TWO

**This chapter deals with the tetrahydrofuran and hydrogen peroxide mediated synthesis and characterization of nanocrystalline Prussian blue nanoparticles having processability for practical applications. As synthesized PBNPs was further characterized through various techniques and used for the detection of hydrogen peroxide in homogeneous and heterogeneous medium.**

# 1 THF and $H_2O_2$ mediated synthesis of nanocrystalline PBNPs and its analytical applications

## 1.1 Introduction

In recent years, Prussian blue and its mixed metal analogues have emerged as a potential tool for the detection of many biological or non biological analytes as a sensing material or as energy storage devices and many more applications [(Sattarahmady and Heli 2011; Yang *et al.* 2012; You *et al.* 2014; Zhang *et al.* 2012a)]. Prussian blue is the simplest member of the family metal hexacyanoferrates and its different analogues have also been synthesized and utilized for the development of chemical/biosensor. Apart of these, nanomaterials are particularly more fascinating since their exceptional physical, chemical, mechanical and electrical properties directed us to use it in the sensing devices and transducers with superior performances.

Among the different synthetic approaches for Prussian blue and its mixed metal analogues, two methods have been used for these purposes. One is single precursor based and another is double precursor based synthesis of Prussian blue and its mixed metal analogues. Double precursor based synthesis of Prussian blue involves two ways. In one ways, equimolar aqueous solution of $K_3[Fe(CN)_6]$ and $FeSO_4$ mixed in the presence of a stabilizer. In other way of synthesis of Prussian blue by double precursor, equimolar mixture of $FeCl_3$ and $K_3[Fe(CN)_6]$ is used. In single precursor based synthesis of Prussian blue involves only $K_3[M(CN)_6]$ or $K_4[M(CN)_6]$ where represents as Co, Fe or other transition metal ions. This method involves the dissociation of single precursor in the surfactant-formed microemulsion system [(Ding *et al.* 2009)]. Preparation of PB and its analogue have been synthesized through various methods including chemical [(Fiorito *et al.* 2005; Hornok and Dékány 2007; Hu *et al.* 2005; Jia and Sun 2007; Xian *et al.* 2007)] and electrochemical [(Karyakin 2001; Karyakin *et al.* 2004; McCormac *et al.* 1996; Zhang *et al.* 2003)]. These studies involved to control the shape and size of Prussian blue nanoparticles through the involvement of either stabilizer, reaction condition like pH of the reaction mixture, temperature or reaction time. The shape and size of nanoparticles depends upon the molar ratio of stabilizer to

precursor and theses can be induced by sonochemical, hydrothermal or illumination process. Smaller size of nanoparticle plays an important role from application point of view, smaller size of particles may enhance the dispersibility in common solvents. This could helps in the utilizing these materials in thin film processing, optical properties, electrochemical behaviour and nanocomposite synthesis. Accordingly, different methodology and stabilizers have been studied and reported around the world [(Fornasieri and Bleuzen 2008; Li *et al.* 2012; Miao and Liu 2016; Wang *et al.* 2016b; Yang *et al.* 2012)]. Therefore, the challenge is to synthesize PBNPs having better crystallinity, dispersibility and nanogeometry. In addition to that functionality of nanoparticles has also been a serious attention.

Now a days, a number of studies have been published based on the synthesis of Prussian blue through the involvement of single source precursor $K_3[Fe(CN)_6]$ [(Hu *et al.* 2005; Jia and Sun 2007; Pandey and Pandey 2013c, 2014a; Wu *et al.* 2006)]. Our research group have also synthesized single precursor based synthesis of Prussian blue nanoparticles [(Pandey and Pandey 2013c, 2014a)]. The Prussian blue obtained from conventional route of chemical synthesis is insoluble in many solvent restricting their use in various practical applications. Accordingly, controlled synthetic protocol leads to the formation of Prussian blue nanoparticles (PBNPs) have been one challenging task. Meeting to these requirements, we have recently demonstrated the role of 3- Aminopropyltrimethoxysilane (3APTMS) and cyclohexanone during controlled synthesis of PBNPs having average size of 15.8 nm which display excellent redox activity with electron transfer rate constant to the order of 32.1 $s^{-1}$ [(Pandey and Pandey 2013c)]. The optimum ratio of potassium ferricyanide, 3-APTMS and cyclohexanone enable the formation of processable PBNPs at room temperature. In addition to that the similar process also enabled the controlled synthesis of mix metal hexacyanoferrate [(Pandey and Pandey 2013a, b, d)]. The disadvantage of the process is limited to the use of 3-APTMS that undergo auto-hydrolysis, condensation and polycondensation thus affecting the properties of PBNPs for many practical applications. Fortunately, we succeeded in replacing the use of 3-APTMS and found that tetrahydrofuran-hydroperoxide (THF-HP) efficiently enable the conversion of potassium

ferricyanide into PBNPs under ambient condition [(Pandey and Pandey 2014a)].The use of THF-HP during controlled synthesis of PBNPs directed us to examine the contribution of tetrahydrofuran (THF) and hydrogen peroxide ($H_2O_2$) during such process. Therefore, this work is based on organic reagent, tetrahydrofuran (THF) and hydrogen peroxide ($H_2O_2$) mediated synthesis of nanocrystalline Prussian blue nanoparticles (PBNPs) with the involvement of sole precursor potassium ferricyanide [$K_3Fe(CN)_6$]. The as synthesized PBNPs were used for the homogeneous and heterogeneous catalysis of $H_2O_2$ sensing.

## 1.2 Experimental

### 1.2.1 Material and Methods

Potassium ferricyanide $K_3[Fe(CN)_6]$ and hydrogen peroxide ($H_2O_2$) were purchased from Merck, India. O-dianisidine, graphite powder, (particle size 1-2 μm) and nujol oil (density-0.838 g $mL^{-1}$) were purchased from Sigma Aldrich Chemicals Co. India. Tetrahydrofuran (THF) was purchased from Alfa Aesar, India. All other chemicals were used of analytical grade. The water used in all the experiments was double distilled water (Alga water purification system).

### 1.2.2 THF and $H_2O_2$ mediated synthesis of nanocrystalline Prussian blue nanoparticles

In a typical procedure, 70 μl aqueous solution of $K_3[Fe(CN)_6]$ (0.05 M) and 10 μl of THF(12 M) were mixed under stirred condition over vertex cyclomixture. Later, 20 μl of $H_2O_2$ (3.5 M) was added and mixed carefully. The resultant mixture was kept at 60 °C for 20 minutes in an oven. The yellow colour solution of $K_3[Fe(CN)_6]$ was turned into deep blue colour solution which indicates the synthesis of PBNPs. PBNPs may be treated with ethyl acetate to eliminate residual organic moiety and collected by centrifugation and dried the precipitate. The optimum concentration of $K_3[Fe(CN)_6]$ / THF and $H_2O_2$ were achieved by varying the concentrations of one component while keeping fixed concentrations of other component.

**Table.2.1.** Characteristics of PBNPs sol as a function of $H_2O_2$ concentration.

| Vial | $K_3[Fe(CN)_6]$ (mol $L^{-1}$) | THF (mol $L^{-1}$) | $H_2O_2$ (mol $L^{-1}$) | PBNPs sol formation | Extent of Formation |
|---|---|---|---|---|---|
| A | 0.025 | 1.20 | 0.03 | Green | + |
| B | 0.025 | 1.20 | 0.06 | Light Blue | ++ |
| C | 0.025 | 1.20 | 0.13 | Light Blue | +++ |
| D | 0.025 | 1.20 | 0.35 | Light Blue | ++++ |
| E | 0.025 | 1.20 | 0.70 | Blue | +++++ |
| F | 0.025 | 1.20 | 1.05 | Blue | +++ |
| G | 0.025 | 1.20 | 1.40 | Light Blue | +++ |

**Table.2. 2.** Characteristics of PBNPs sol as a function of THF concentration.

| Vial | $K_3[Fe(CN)_6]$ (mol $L^{-1}$) | THF (mol $L^{-1}$) | $H_2O_2$ (mol $L^{-1}$) | PBNPs sol formation | Extent of Formation |
|---|---|---|---|---|---|
| A | 0.025 | 0.15 | 0.7 | Light Green | + |
| B | 0.025 | 0.31 | 0.7 | Light Blue | +++ |
| C | 0.025 | 0.62 | 0.7 | Light Blue | +++ |
| D | 0.025 | 1.20 | 0.7 | Blue | +++++ |

| | | | | | |
|---|---|---|---|---|---|
| E | 0.025 | 2.40 | 0.7 | Light Blue | ++++ |
| F | 0.025 | 3.69 | 0.7 | Light Blue | ++++ |
| G | 0.025 | 4.93 | 0.7 | Light Blue | ++++ |

**Table.2.3.** Characteristics of PBNPs sol as a function of $K_3[Fe(CN)_6]$ concentration.

| Vial | $K_3[Fe(CN)_6]$ (mol $L^{-1}$) | THF (mol $L^{-1}$) | $H_2O_2$ (mol $L^{-1}$) | PBNPs sol formation | Extent of Formation |
|---|---|---|---|---|---|
| A | 0.003 | 1.20 | 0.7 | -ve | - |
| B | 0.007 | 1.20 | 0.7 | Light Blue | ++ |
| C | 0.015 | 1.20 | 0.7 | Light Blue | ++ |
| D | 0.025 | 1.20 | 0.7 | Light Blue | +++ |
| E | 0.035 | 1.20 | 0.7 | Blue | +++++ |
| F | 0.045 | 1.20 | 0.7 | Light Blue | ++ |

### 1.2.3 Measurement and characterization

The absorbance spectra of samples were recorded using a Hitachi U-2900 spectrophotometer. The PB-powder was made by drying the PBNPs suspension at 50 C for an overnight. A Perkin Elmer spectrum 100 spectrometer was used for Fourier Transform Infrared (FT-IR) measurements with spectral range limited to 4,000–500 $cm^{-1}$. Energy dispersive spectroscopic (EDS) analysis was conducted

with ZEISS SUPRA 40 Scanning Electron Microscope (SEM) coupled to an Energy Dispersive spectrometer. The X-ray diffraction pattern of Prussian blue powder was obtained on Rigaku miniflex II diffractometer, using CuKα (λ = 1.506 Å) radiation. Crystallite size was calculated from the characteristic peaks obtained from X-ray diffractogram at 17.3° (200), 24.9° (220), 35.0° (400) and 39.6° (420) (2θ value) using Debye-Scherrer formula [(Zheng *et al.* 2007)] as:-

$$D = \frac{0.9\,\lambda}{\beta\,cos\theta}$$

Where

- λ is the wavelength of X-rays,
- β is the line broadening at half the maximum intensity,
- θ is the Bragg angle,
- 0.9 is the dimensionless shape factor, with a value close to unity.

Transmission Electron Microscopy (TEM) study was performed using TECNAI 200 kV TEM (Fei, Electron Optics) microscope (Tokyo, Japan) operational voltage 200 kV Electrochemical experiments were performed on an electrochemical workstation Model CHI660, CH Instruments Inc., TX, and USA, in a three electrode configuration with a working volume of 3 ml. An Ag|AgCl electrode (Orion, Beverly, MA, USA) and a platinum plate electrode functions as reference and counter electrodes respectively. All potentials given in text are relative to the Ag|AgCl reference electrode. Graphite paste electrode (GPE) worked as a working electrode.

### 1.2.4 Peroxidase like catalytic activity of Prussian blue nanoparticles

Peroxidase like catalytic activity of as synthesized Prussian blue nanoparticle solution was measured as described earlier [(Pandey and Panday 2016b)]. In a typical situation, peroxidase like activity of as synthesized PBNPs was determined spectrophotometrically by measuring the oxidised product of o-dianisidine at 430 nm (ε = 11.3 $mM^{-1}$ $cm^{-1}$) using Hitachi U-2900 spectrophotometer. Peroxidase like activity was measured by probing the

formation of oxidation product of o-dianisidine in 0.1 M phosphate buffer (pH=7.0) in the presence of varying concentration of $H_2O_2$ (0–14 mM) and 50 μM o-dianisidine at 25 °C keeping constant concentration of PBNPs (15 μL $ml^{-1}$). The steady state kinetics was performed by varying the concentration of $H_2O_2$ (0–14 mM) at fixed concentration of o-dianisidine (50 μM). The reaction was conducted in 2 ml phosphate buffer (0.1 M, pH=7.0) and the variation of absorbance was monitored as function of time at 430 nm (ε = 11.3 $mM^{-1}$ $cm^{-1}$). The kinetic parameters were calculated by fitting the absorbance data to the Michaelis-Menten equation.

$$V = V_{max} [C]/K_m + [C] \quad (1)$$

Where V is the rate of conversion, $V_{max}$ is the maximal reaction velocity, C is the concentration of the substrate, and $K_m$ is the Michaelis-Menton constant.

### 1.2.5 Preparation of modified graphite paste electrode

Preparation of active paste of PBNPs made through THF and $H_2O_2$: Active paste of PBNPs was made by mixing 200 μl of PBNPs solution with 100 mg spectroscopic grade graphite powder. Mixed properly and followed by ultrasonication for 30 minutes and left to dry 60 °C in a vacuum oven overnight. Graphite paste electrode was functioned as working electrode used for electrochemical measurement. Electrode body was purchased from Bioanalytical systems (West Lafayette, In (MF 2010). The well of electrode was filled with an active paste of composition as graphite powder = 68 % (w/w), active paste = 2.5 % (w/w) and nujol oil = 30 % (w/w). The desired amount of modifier was thoroughly mixed with graphite powder (particle size 1-2 μm) in a blender and addition of nujol oil. The paste surface was manually smoothed on a clean butter paper.

## 1.3 Results

### 1.3.1 THF and $H_2O_2$ mediated synthesis of nanocrystalline PBNPs

THF and $H_2O_2$ mediated synthesis of PBNPs was characterized by UV-Vis spectroscopy and simple photoimaging. At first instance, we tried to understand the importance of each component i.e., $K_3[Fe(CN)_6$, THF and $H_2O_2$ and the result

is shown in Figure.2.1 in which the UV-Vis spectroscopy is shown along with their vial photographs.

The optimum concentration of each component was investigated by varying the one component concentration while keeping the other component concentration constant. Figure.2.2 shows the constant concentration of THF (1.2 M) and $K_3[Fe(CN)_6]$ (25 mM) and varying concentration of $H_2O_2$ (0.03 M to 1.40 M). The inset to each figure depicts the photographs of corresponding UV-Vis spectra (Table.2.1).

Figure.2.2 shows the systems containing constant concentrations of $K_3[Fe(CN)_6]$ (25 mM) and $H_2O_2$ (0.70 M) and varying concentrations of THF (0.15 M to 4.5 M). The inset to each figure shows the photographs of corresponding UV-Vis spectra (Table.2.2). Similarly, Figure.2.3. shows the UV-Vis spectra of systems containing constant concentrations of THF (1.2 M) and $H_2O_2$ (0.7 M) and varying concentration of $K_3[Fe(CN)_6]$ (3 mM to 45 mM). The inset to the each figure represents the visual photograph of corresponding vial (Table.2.3). Figure.2.1.(E) and Figure.2.2.(D) represents the optimum concentrations of THF and $H_2O_2$ while Figure.2.3.(E) represents the optimum concentration of $K_3[Fe(CN)_6]$ required for the synthesis of PBNPs having admirable absorption maxima at 680 nm and represents the optimum compositions.

Structural characterization of as synthesized PBNPs was done by FT-IR, XRD, EDS and TEM analysis.

As synthesized PBNPs was further characterized by FTIR. Figure.2.5 represents the FT-IR spectra of as synthesized PBNPs. The spectrum shows the strong absorption at 2090 $cm^{-1}$ and in addition to that other bands at 3400 $cm^{-1}$ and 1600 $cm^{-1}$.

In order to further characterize the PBNPs, XRD analysis was done using powder sample and the diffractogram is shown in Figure.2.6 There are four major diffraction characteristic peaks at c.a. 17.3°, 24.9°, 35.0° and 39.6° (2θ values). The crystallite size was calculated by using Scherrer formula. EDS analysis was performed to know the element present in the as synthesized material. Figure.2.7

shows the EDS analysis spectra and the inset shows the percentage of the element present in the samples. Transmission Electron Microscopy (TEM) was done to know the particles size. Figure.2.8 shows the TEM image of PBNPs depicts that the particle size ranges between 30 nm to 40 nm.

### 1.3.2 Electrochemical characterization of as synthesized PBNPs

The electrochemical characterization of PBNPs was done with the carbon paste modified electrode. Figure.2.9. (A) shows the cyclic voltammogram of as synthesized PBNPs modified electrode in 0.1 M $KNO_3$ as supporting electrolyte at increasing scan rate between 0.01 V $s^{-1}$ to 0.3 V $s^{-1}$. Two reversible redox couples were observed for PBNPs modified electrode between the potential ranges of -0.2 V to 1.0 V *vs*. Ag|AgCl reference electrode. Figure.2.9. (B) shows the cyclic voltammogram of as synthesized PBNPs at scan rate 0.01 $Vs^{-1}$ in 0.1 M $KNO_3$ as supporting electrolyte. An analysis of the electrochemical behaviour of PBNPs was performed from the plot of peak current density (j) *vs*. scan rate (ν) of the PB/PW redox couples in the range of -0.2 V to 0.5 V *vs.* Ag|AgCl [Figure.2.9. (C)]. Figure. 2.9. (D) shows the plot of peak current density *vs.* square root of scan rate for PBNPs.

### 1.3.3 Peroxidase like activity of PBNPs made through THF and $H_2O_2$

It is necessary to study the peroxidase mimetic behaviour of PBNPs made through THF and $H_2O_2$. Accordingly, attempt has been made to investigate the peroxidase mimetic activity of the same towards the oxidation of o-dianisidine. Catalytic activity of PBNPs is $H_2O_2$ concentration dependent; this can be used to detect $H_2O_2$. The results on time dependent absorbance changes at 430 nm in the presence of different concentration of $H_2O_2$ and fixed concentration of o-dianisidine catalyzed by PBNPs as shown in Figure.2.11 and the subsequent $K_m$ and $V_{max}$ value of PBNPs for $H_2O_2$ analysis was calculated from graph as shown in Figure.2.12.

### 1.3.4 Electrocatalytic reduction of $H_2O_2$ on the PBNPs modified electrode

Reduction of $H_2O_2$ was performed on graphite paste modified electrode in 0.1 M phosphate buffer containing 0.5 M KCl (pH=7.0) in a three electrode assembly system. The cyclic voltammograms of $H_2O_2$ reduction over PBNPs modified electrode is shown in Figure.2.13. The finding was further supported by experimental observation based on amperometry. Figure.2.14 shows the typical amperometric response of PBNPs on the successive additions of $H_2O_2$ in 0.1 M phosphate buffer (pH=7.0) containing 0.5 M KCl at fixed potential of 0.0 V. Successive additions of $H_2O_2$ resulted in the increase in the reduction current showing the catalytic property of modified electrode. Inset to the Figure.2.14 shows the calibration plot for $H_2O_2$ determination and shows that the linearity range 0.5 μM to 2000 μM and the lowest detection limit is 0.1 μM (S/N = 3). The sensitivity for $H_2O_2$ analysis was found to be 156.5 μA $mM^{-1}$ $cm^{-2}$.

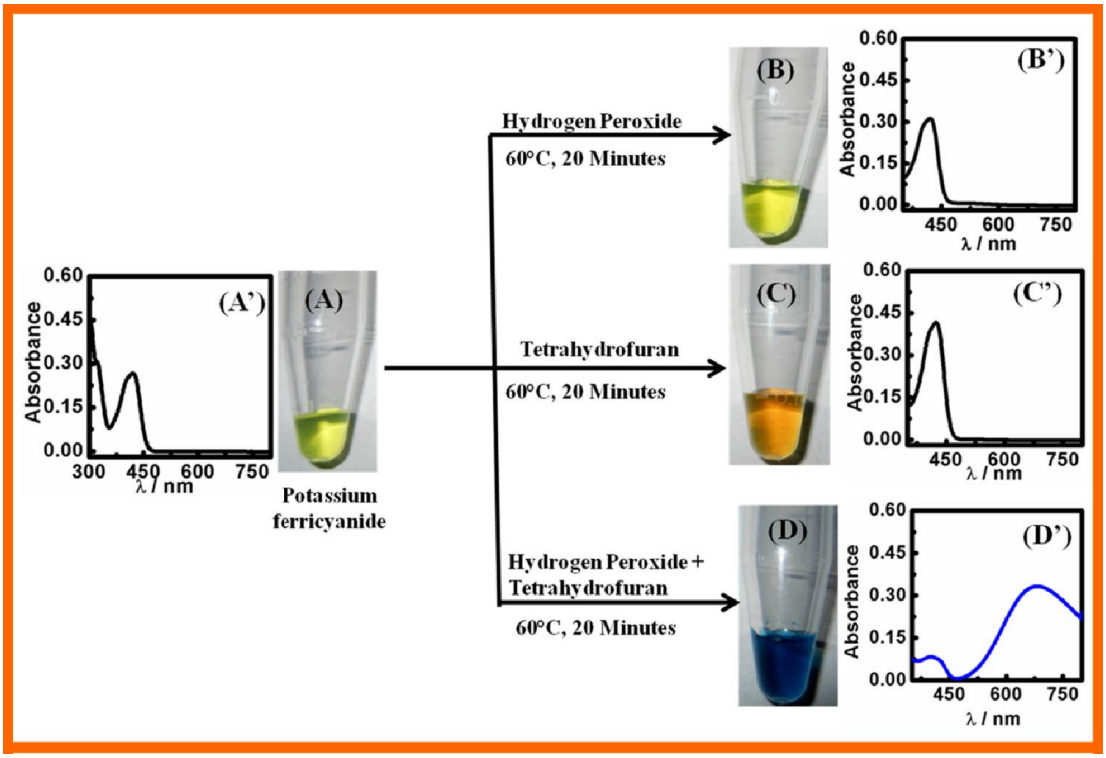


**Figure.2.1.** Schematic presentation of synthesis of PBNPs from optimum concentration of $K_3[Fe(CN)_6]$, THF and $H_2O_2$.

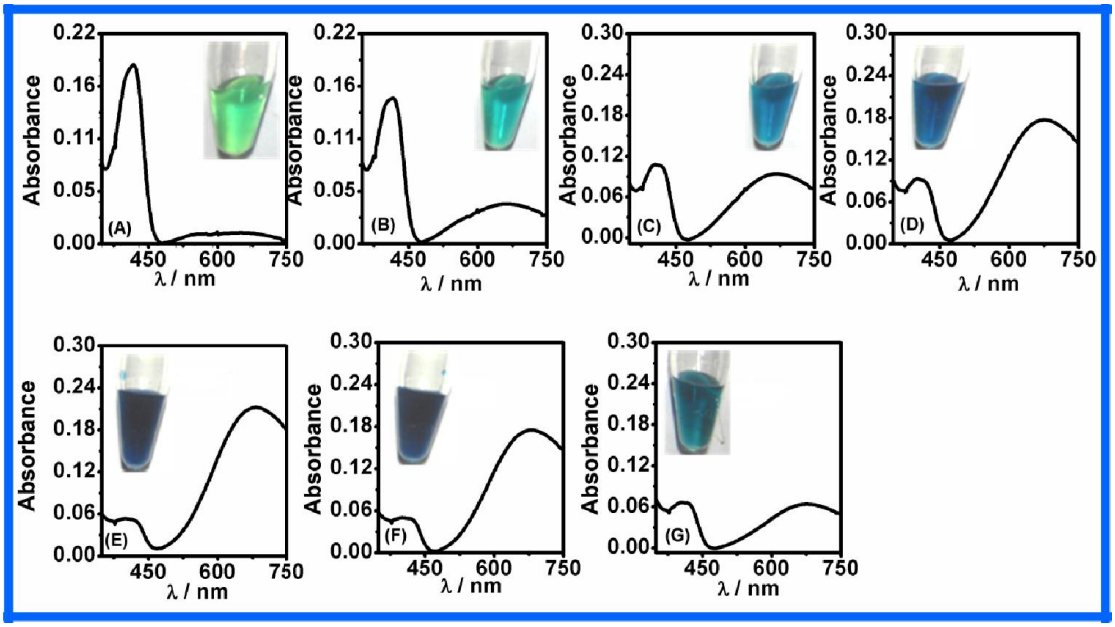


**Figure.2.2.** UV–Vis spectra of systems containing constant concentration of THF (1.2 M) and $K_3[Fe(CN)_6]$ (25 mM) and the varying concentration of $H_2O_2$ (from 0.003 M to 1.40 M). The corresponding vial visual photographs are shown in the inset of the respective systems.

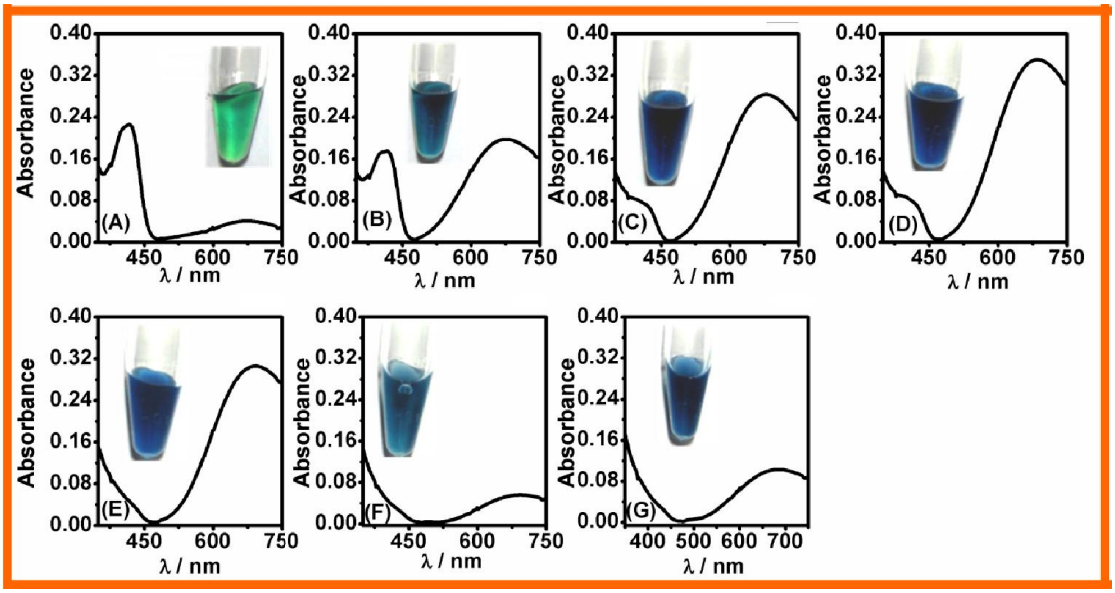


**Figure.2.3.** Systems containing constant concentration of $K_3[Fe(CN)_6]$ (25 mM): and $H_2O_2$ (0.70 M): and varying concentration of THF (from 0.15 M to 4.5 M). The corresponding vial visual photographs are shown in the inset of the respective systems.

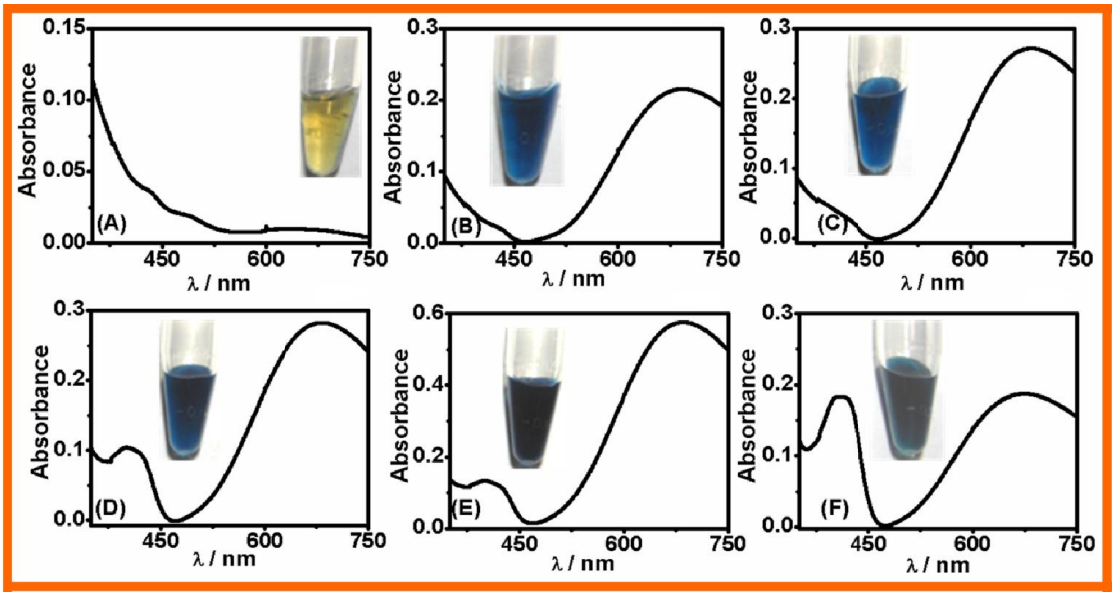


**Figure.2.4.** Systems containing constant concentration of THF (1.2 M) and $H_2O_2$ (0.7 M): and varying concentration of $K_3[Fe(CN)_6]$ (from 3 mM to 45 mM): The corresponding vial visual photographs are shown in the inset of the respective systems.

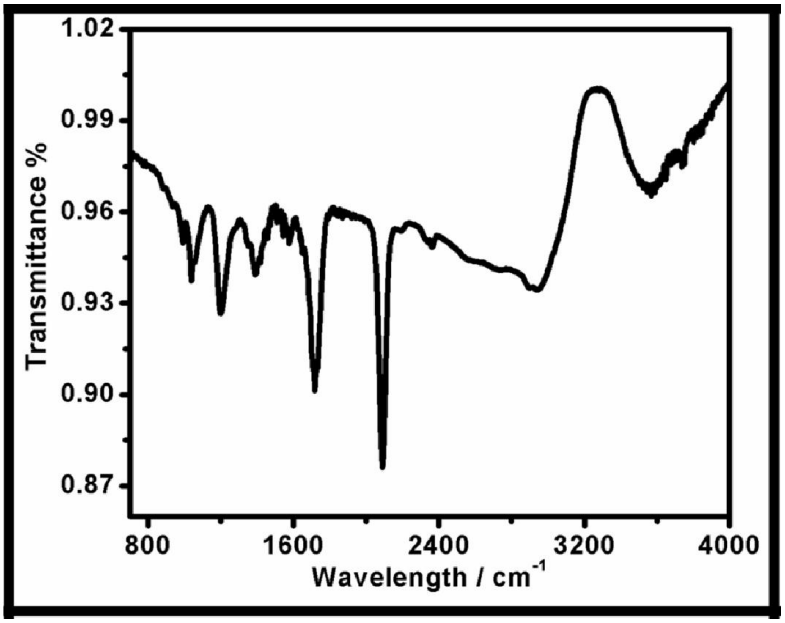


**Figure.2.5.** FT-IR spectra of THF and $H_2O_2$ mediated synthesized PBNPs.

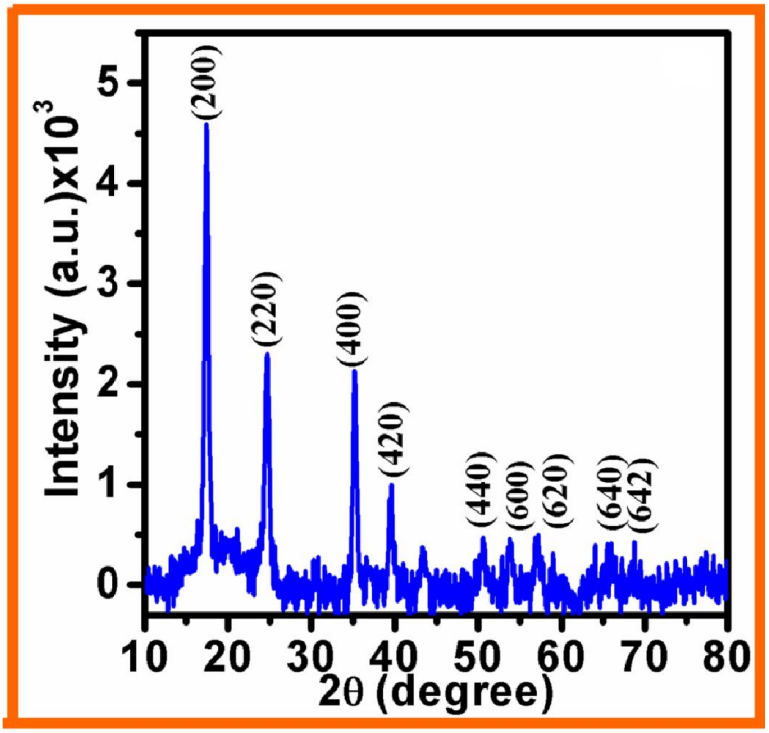


**Figure.2.6.** XRD pattern of THF and $H_2O_2$ mediated synthesized PBNPs.

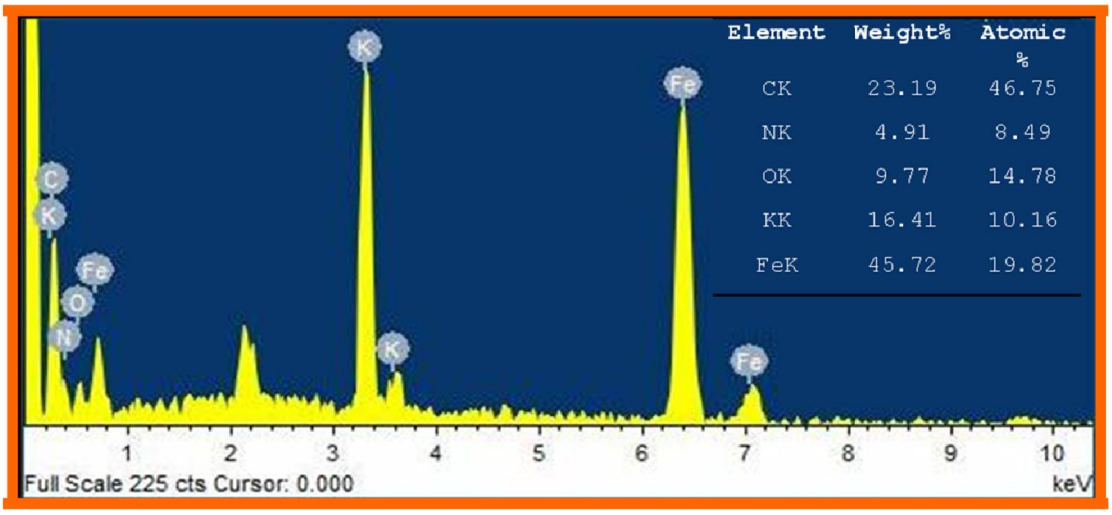


**Figure.2.7.** EDS spectra of THF and $H_2O_2$ mediated synthesized of PBNPs.

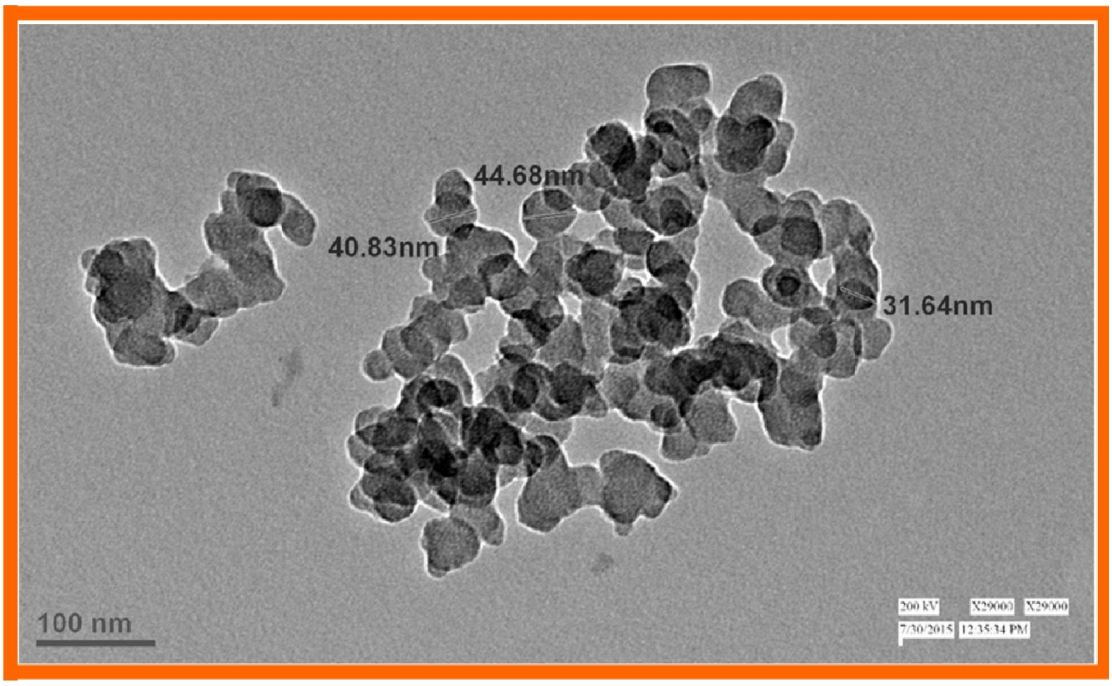


**Figure.2.8.** TEM image of THF and $H_2O_2$ mediated synthesized of PBNPs.

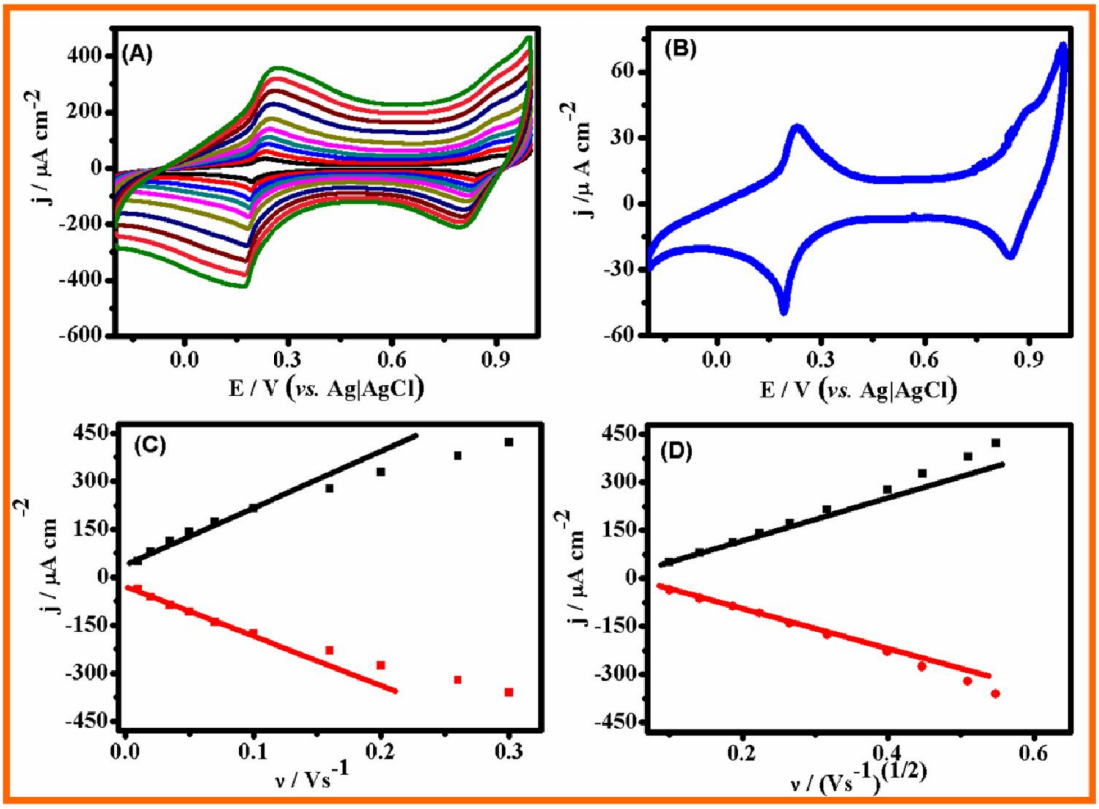


**Figure.2.9.** (A) Cyclic voltammograms of THF and $H_2O_2$ mediated synthesized PBNPs in 0.1 M $KNO_3$ at various scan rates between 0.01 V $s^{-1}$ and 0.3 V $s^{-1}$. (B) A typical voltammogram of THF and $H_2O_2$ mediated synthesized PBNPs at scan rate 0.005 V $s^{-1}$. (C) The plots of peak current density vs. scan rate for PBNPs. (D) the plots of peak current density *vs.* square root of scan rate for PBNPs.

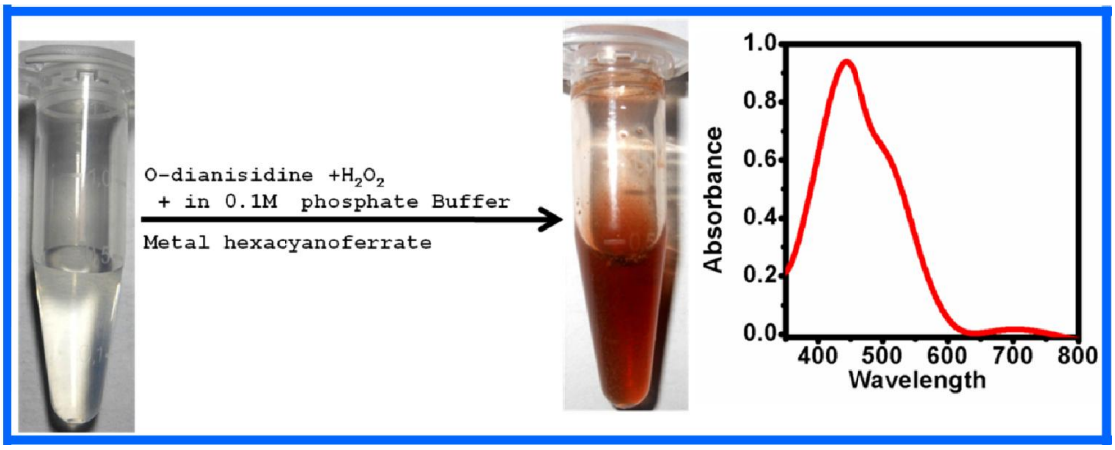


**Figure.2.10**. Colour conversion of o-dianisidine and $H_2O_2$ in the presence of metal hexacyanoferrates.

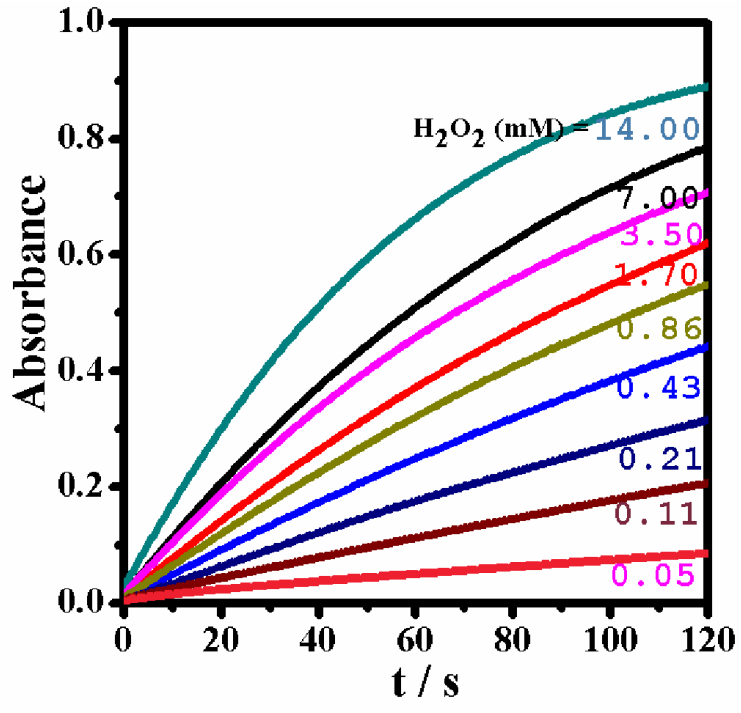


**Figure.2.11.** Time dependent absorbance changes at 430 nm in the presence of different concentrations of $H_2O_2$ (from 0.05 mM to 14 mM and fixed concentration of o-dianisidine (50 µM) catalyzed by PBNPs.

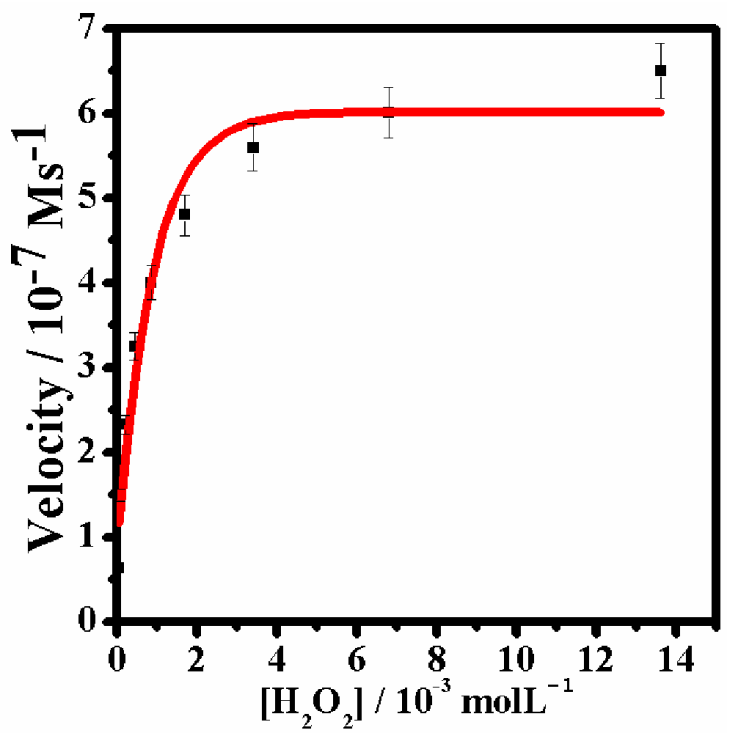


**Figure.2.12.** Kinetic analysis of PBNPs with $H_2O_2$ as substrate.

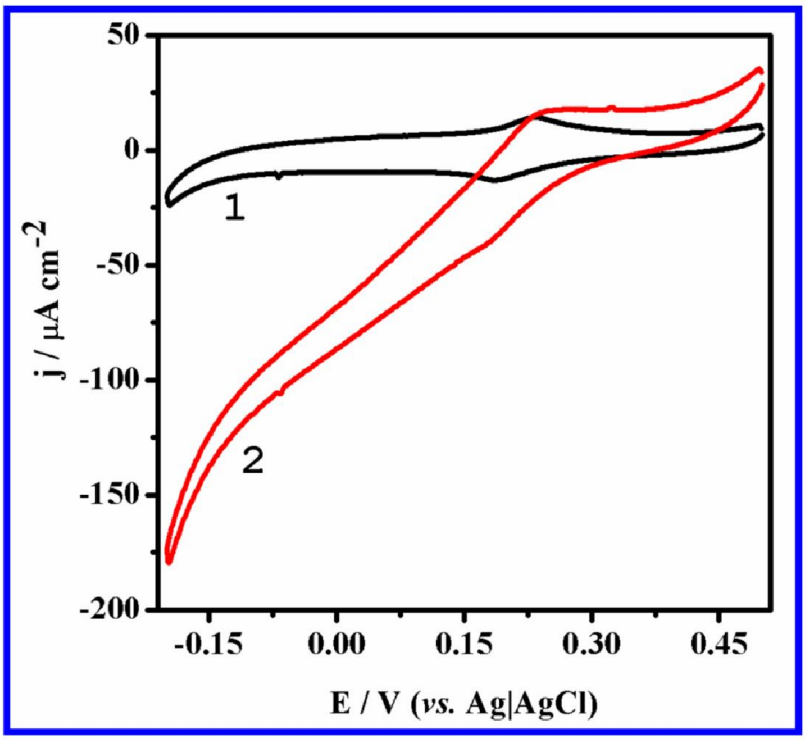


**Figure.2.13.** Cyclic voltammograms of PBNPs modified electrode in the absence (1) and the presence (2) of 1 mM $H_2O_2$ in 0.1 M phosphate buffer pH=7.0 containing 0.5 M KCl.

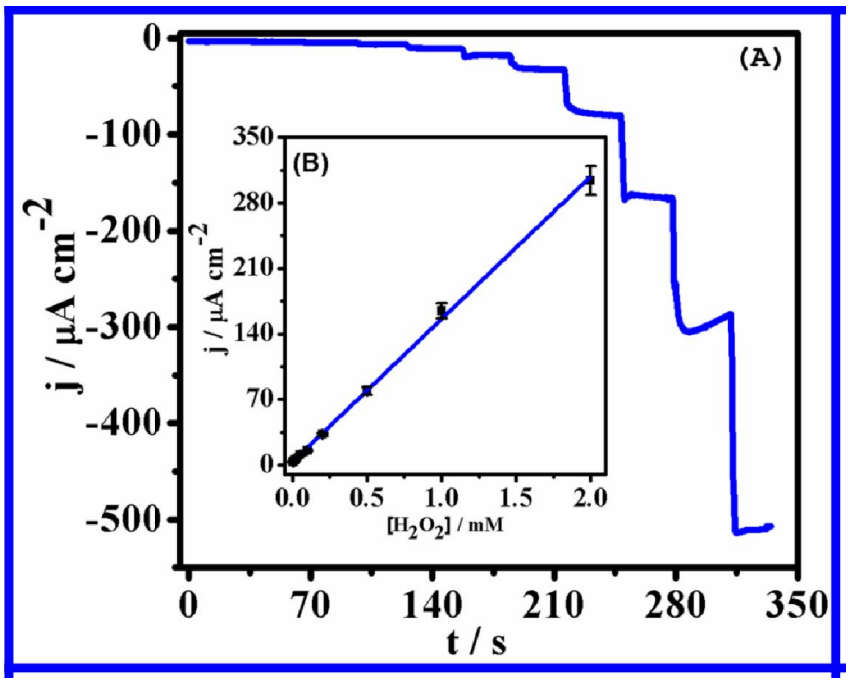


**Figure.2.14.** Amperometric response of PBNPs modified electrode on the addition of varying concentrations of $H_2O_2$ between 0.01 mM and 5 mM; operating potential, 0.0 V; 0.1 M phosphate buffer (pH=7.0) containing 0.5 M KCl as supporting electrolyte, The inset (B) shows calibration plots for PBNPs.

## 1.4 Discussion

The crystallinity, nanogeometry and processability of Prussian blue are the pre-requisites, lack of which has restricted the practical application of PBNPs. Previously, we have attempted to synthesize Prussian blue nanoparticles (PBNPs) mediated through tetrahydrofuran-hydroperoxide (THF-HP) at room temperature in 12 hours. THF-HP also allowed the formation of gold and palladium nanoparticles [(Pandey and Pandey 2014b; Pandey *et al.* 2014b)]. However, the synthesis of THF-HP has been a difficult task. Accordingly, attempt has been made to synthesize PBNPs mediated through easily available laboratory chemicals i.e., tetrahydrofuran (THF) and hydrogen peroxide ($H_2O_2$) and we got the positive result.

We found that THF and $H_2O_2$ converts single precursor $K_3[Fe(CN)_6]$ into stable, well dispersed PBNPs at 60 °C in 20 minutes. At first, we tried to understand the role of each reagent i.e., THF, $H_2O_2$ and $K_3[Fe(CN)_6]$. Figure.2.1. demonstrates the role of each component (THF and $H_2O_2$) during the proposed reaction protocol. The findings justified that neither THF nor $H_2O_2$ alone enable the conversion of $K_3[Fe(CN)_6]$ into PBNPs [Figure.2.1(B) and Figure.2. 1(C)] however when both THF and $H_2O_2$ are mixed together with $K_3[Fe(CN)_6]$, controlled formation of PBNPs at 60 °C within < 20 minutes was recorded [Figure. 1(D)]. As we can see from the Figure.2.1. in UV-Vis spectroscopy, when all the three components are present in the reaction system then a characteristic peaks of $K_3[Fe(CN)_6]$ at 420 nm has decreased and a characteristic peaks of Prussian blue at 680 nm is emerged. This justified that all the three components are required for the efficient conversion of $K_3[Fe(CN)_6]$ into PBNPs.

The conversion of $K_3[Fe(CN)_6]$ mediated through THF and $H_2O_2$ can be represented as following reaction mechanism as shown in scheme.2.1.

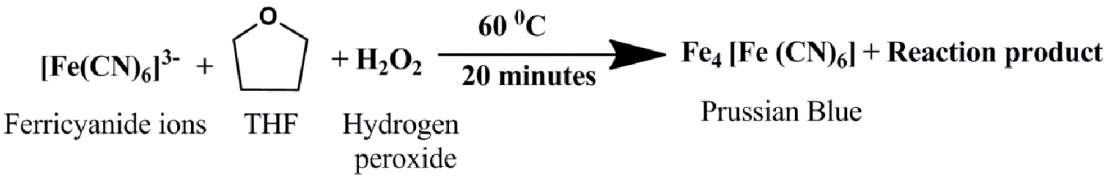


**Scheme.2.1.** Scheme for THF and $H_2O_2$ mediated synthesis of PBNPs.

The process of conversion of single precursor $K_3[Fe(CN)]_6$ to the PBNPs may involve the following steps:

i. Some ferricyanide ions breaks and forms some $Fe^{3+}$ ions and some undissociated ferricyanide ions to obtain $Fe^{2+}$ ions
ii. The undissociated ferricyanide ions and $Fe^{3+}$ ions may lead to the formation of Prussian blue nanoparticles.

### 1.4.1 Optimization of THF and $H_2O_2$ mediated synthesis of nanocrystalline PBNPs

The optimum concentration of each component was investigated based on UV-Vis spectroscopy and the visual photographs of the corresponding vials. The optimum concentration of THF, $H_2O_2$ and $K_3[Fe(CN)_6]$ required for best PBNPs formation was achieved by varying the concentrations of one component while keeping fixed concentrations of other two components as shown in Table.2.1-Table.2.3.

Figure.2.2. shows the UV-Vis spectra of systems containing constant concentration of $K_3[Fe(CN)_6]$ and THF and varying concentration of $H_2O_2$ (0.03 M to 0.7 M). Inset to the Figure.2.2. shows the photographs of PBNPs sol of the respective graphs.

Figure.2.3. shows the UV-Vis spectra of systems containing constant concentration of $K_3[Fe(CN)_6]$ and $H_2O_2$ and the varying concentration of THF (0.15 M to 1.20 M). Inset to the Figure.2.3. shows the photographs of PBNPs sol of the respective graphs.

Figure.2.4. shows the UV-Vis spectra of THF and $H_2O_2$ and varying concentration of $K_3[Fe(CN)_6]$ (3 mM to 45 mM). Inset to the Figure.2.3. shows the photographs of PBNPs sol of the respective graphs.

As we can see from the Figure.2.4.(E) is best optimum concentrations of each component in which the absorbance value at 420 nm (characteristic peak of potassium ferricyanide) is low and at 680 nm (characteristic peak of PB) is the maximum.

### 1.4.2 Characterization of THF and $H_2O_2$ mediated synthesized nanocrystalline PBNPs

As synthesized PBNPs was characterized through various techniques like Fourier Transform Infrared spectroscopy (FT-IR), X-ray diffraction spectroscopy (XRD), Energy Dispersive Spectroscopy (EDS) analysis and Transmission Electron Microscopy (TEM).

#### *1.4.2.1 FT-IR analysis*

As synthesized PBNPs was characterized by Fourier Transformation Infrared Spectroscopy (FT-IR). Figure.2.5. shows the strong absorption peak at 2090 $cm^{-1}$ which is the common characteristic peaks of PBNPs and its mixed metal analogues, corresponds to the stretching vibration of the cyano group [(Ayers and Waggoner 1971; Wilde *et al.* 1970)]. In addition to that, the broad absorption peaks near 3,400 $cm^{-1}$ and 1,600 $cm^{-1}$ refers to the O-H stretching mode and H-O-H bending mode respectively, indicating the presence of interstitial water in the sample [(Itaya *et al.* 1986)].

#### *1.4.2.2 XRD analysis*

PBNPs was also characterised by X-ray diffraction analysis. Figure.2.6. shows the X-ray diffractogram of as synthesized PBNPs. There are four major characteristic peaks at c.a. 17.3°, 24.9°, 35.0° and 39.6° (2θ values) that can be assigned to the PB phase (200), (220), (400) and (420) crystal planes respectively. In addition to these characteristic peaks, few peaks are also available at c.a. 50.5°, 53.8°, 57.2°, 65.9° and 68.7° (2θ value) that can be assigned to the PB phase of (440), (600), (620), (640) and (642) respectively [JCPDS file No- 073-0687]. The crystallite size, which was determined from the half-width of the diffraction peaks by using Scherrer formula [(Zheng *et al.* 2007)] at different characteristic peaks which were found as 14.06 nm, 10.05 nm, 13.32 nm and 14.20 nm respectively.

#### *1.4.2.3 EDS and TEM analysis*

For elemental analysis of as synthesized PBNPs, Energy Dispersive Spectroscopy (EDS) was done. Figure.2.7. shows the EDS spectrum which

indicates the presence of characteristic peaks assigned to carbon, nitrogen, potassium and iron. The percentage of the respective element is shown in the inset to the Figure.2.7.

As synthesized PBNPs were characterized by Transmission Electron Microscopy (TEM) to evaluate the particle size of nanocrystalline material. Figure.2.8. shows the TEM photograph of the as synthesized PBNPs. The particle size of the PBNPs lies in the range of 30 nm to 40 nm. The shapes of the nanoparticles are spherical in nature however the agglomeration of nanoparticles may occur that justify the variation in nanogeometry calculated from TEM and XRD analysis. In addition to that, the particle size calculated from TEM images may be higher than the value obtained from XRD analysis since the size obtained from the TEM analysis is particle size while the size obtained from XRD pattern is crystallite size similar to that reported earlier [(Agnihotri *et al.* 2014; Wang *et al.* 2007c; Zheng *et al.* 2007)].

### 1.4.3 Electrochemical analysis of THF and $H_2O_2$ mediated synthesized PBNPs

Electrochemistry of PBNPs have been performed for many workers and the results are demonstrated the applicability of PBNPs. Electrochemical behaviour of PBNPs electrode was studied through cyclic voltammetry to confirm the synthesis of PBNPs and redox behaviour. The cyclic voltammetry was done by the graphite paste electrode in 0.1 M $KNO_3$ at increasing scan rate between 0.01 $Vs^{-1}$ to 0.3 $Vs^{-1}$ [Figure.2.9 (A)]. There are two reversible redox peaks were present between the potential range of -0.2 V to 1.0 V *vs.* Ag|AgCl reference electrode [Figure.2.9 (A) and (B)]. An electrochemical behaviour of as synthesized PBNPs was done from the plot of peak current density (j) *vs*. scan rate (v) of the PB/PW redox couples in the range of -0.2 V to 0.3 V *vs.* Ag|AgCl. In order to understand the charge transport characteristics within the reaction layer, the cathodic and anodic peak current density was plotted against the scan rate and the square root of scan rate. Voltammograms clearly shows the two reversible redox couples between the potential ranges of -0.2 V to 1.0 V *vs*. Ag|AgCl. The first redox couple corresponds to the oxidation of Prussian white and the reduction of Prussian blue.

The second redox couple corresponds to the oxidation of PB and the reduction of PW [(Ricci and Palleschi 2005)].

The effect of scan rate on the cathodic and anodic peak current density (j) was done in the range of 0.2 V to 0.3 V *vs.* Ag|AgCl [Figure.2.9. (C) and (D)]. Results justified that peak current density (j) linearly increases with the scan rate of 0.1 V $s^{-1}$ indicating the charge transport from a surface-confined redox species [Figure.2.9. (C)]. At higher scan rate, peak current density (j) was found to vary linearly with the square root of scan rate ($v^{1/2}$) indicating the change in the reaction kinetics to a diffusion limited process [Figure.2.9. (D)].

### 1.4.4 Peroxidase like activity of PBNPs

Enzymes have been used to catalyze many physiological reactions. Their catalytic efficiency and specificity is very high but the problem is their stability. Enzymes are very susceptible to their local environment like harsh pH, temperature and salt tolerance because of their denaturation. Isolation and purification of enzymes are also expensive. Because of this, other material is required which can work as enzyme and not in proteinaceous in nature which can overcome these drawbacks. In last decades, researchers have been trying to utilize the nanoparticles as enzyme called as enzyme mimetics. Nanoparticles are very popular as enzyme mimetics as they have potentiality for bio-signal magnification (due to its large surface to volume ratio), high catalytic activity and low cost synthesis. Recently, it has been reported that many metal nanoparticles exhibits the intrinsic peroxidase like activity, proved their use as a peroxidase substitute [(Chen *et al.* 2011; Fan *et al.* 2011; Gao *et al.* 2007; Pandey *et al.* 2014a; Wan *et al.* 2012)]. In line of this, Prussian blue or in combination with other composite material was used to enhance the peroxidase mimetic activity [(Pandey and Pandey 2013d; Pandey *et al.* 2014a; Pandey *et al.* 2014b; Zhang *et al.* 2014; Zhang *et al.* 2013)]. Although, there is the challenging demand to enhance the catalytic efficiency of such nanomaterial to the equivalent of biocatalytic activity thereby allowing the precise control of the mimetic character and ultimately leading to the development of new material as a powerful peroxidase *i.e.*, Horseradish peroxidase (HRP) replacement during enzyme and immunosensor

development. These studies motivated us to analyse our material as a peroxidase mimetics. So, we checked peroxidase like activity of as synthesized PBNPs. Accordingly, the present part is focussed on the investigation of peroxidase like behaviour of PBNPs based on the probing of PBNPs with the o-dianisidine-$H_2O_2$ chromogenic reaction as shown below in scheme.2.2.

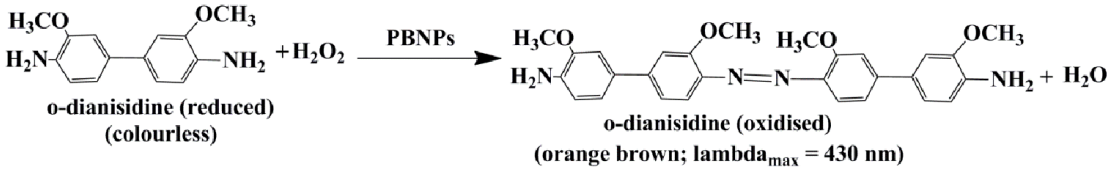


**Scheme.2.2.** Schematic presentation of colorimetric detection of $H_2O_2$ using PBNPs catalyzed colour reaction.

Figure.2.10. shows the UV-Vis spectra of the reaction system containing o-dianisidine, $H_2O_2$ and metal hexacyanoferrates which clearly shows that an increase in absorbance at 430 nm corresponds to the orange brown colour of the oxidised product of o-dianisidine indicating the peroxidase-like activity of the metal hexacyanoferrates.

The peroxidase like activity of as synthesized PBNPs was determined spectrophotometrically by measuring the formation of the oxidised product of o-dianisidine at 430 nm, using a Hitachi U-2900 spectrophotometer. In general, the o-dianisidine formation was measured in 2 ml, 0.1 M phosphate buffer (pH=7.0) containing 50 μM o-dianisidine and PBNPs (15 μL $mL^{-1}$) acted as peroxidase mimetic catalytic material. UV-Vis spectroscopy with time scan mode was used to evaluate the kinetic activity of as synthesized PBNPs. The steady state kinetic was obtained by varying the concentration of $H_2O_2$ while keeping the o-dianisidine concentration constant.

To investigate the apparent steady-state reaction rates, time scan was started as quickly as possible and the absorbance variation with time was monitored at 430 nm. The kinetic parameters of all the materials were evaluated by the initial rate method. The absorbance data were converted to corresponding concentration terms by using the value $\varepsilon = 11.3\ mM^{-1}\ cm^{-2}$ (at 430 nm) for the oxidised product of o-dianisidine. Apparent steady-state reaction rates at different concentration of

$H_2O_2$ as a substrate were obtained by calculating the slopes of initial absorbance changes with time at fixed concentration of MHCFs. It was found that over a certain concentration ranges of $H_2O_2$, the plot of initial rate *vs*. $H_2O_2$ concentration show typical Michaelis-Menton equation. Michaelis- Menton constant ($K_m$) is an indicator of enzyme affinity for its substrate. A high value of $K_m$ indicates the weaker affinity whereas a low value of $K_m$ implies a higher affinity of substrate to enzyme. Figure.2.11. and Figure.2.12. shows the steady state kinetic parameters of as synthesized PBNPs. The apparent $K_m$ value of as synthesized PBNPs was found to be 0.49 mM (Figure.2.12.) where as it was 3.7 mM for HRP as compared from the previous study and justifies the perfect material for the peroxidase replacement in the biochemical reactions. The maximal reaction velocity was found to be 6.03 x $10^{-7}$ $Ms^{-1}$ (Figure.2.12).

### 1.4.5 Electrocatalytic reduction of hydrogen peroxide over THF, $H_2O_2$ mediated synthesized PBNPs modified graphite electrode

$H_2O_2$ itself is considered as a chemical threat agent present in rain and ground water as a waste product of industry and atomic power stations. $H_2O_2$ is the most valuable marker for oxidative stress, recognized as one of the major risk factors in progression of disease-related patho-physiological complications in diabetes, atherosclerosis, renal disease, cancer, aging, and other conditions. Hydrogen peroxide is also a side product of oxidase enzymes which are used in the majority of enzyme-based biosensors and analytical kits like glucose oxidase, horse radish peroxidase *etc*. PBNPs are well known material for catalytic reduction of $H_2O_2$ in a homogeneous and heterogeneous medium. Prussian blue is also known as artificial peroxidase since it facilitates the reduction of $H_2O_2$ at relatively low over potentials analogous to that of peroxidase enzyme.

Electrocatalytic reduction of $H_2O_2$ over PBNPs was performed on the graphite paste electrode in phosphate buffer (0.1 M containing 0.5 M KCl, pH=7.0) in a three electrode assembly system. Cyclic voltammogram in the presence and absence of $H_2O_2$ reduction over PBNPs is shown in Figure.2.13. Figure shows the cyclic voltammograms of PBNPs modified electrode in absence (curve 1) and the presence (curve 2) of 1 mM $H_2O_2$ respectively. As can be seen in the figure, the

cathodic current is started increasing from 0.2 V to negative potential. The finding was further supported by the experimental observation of amperometry. Figure.2.14. shows the amperometric response of PBNPs on the successive addition of $H_2O_2$ in 0.1 M phosphate buffer (pH=7.0) containing 0.5 M KCl under continuous stirred condition at an applied potential of 0.0 V *vs*. Ag|AgCl. Successive addition of $H_2O_2$ leads to the significant increase in the reduction current, showing the catalytic property of the modified electrode to the reduction of $H_2O_2$. The inset to the Figure.2.14. shows the calibration plot of PBNPs. The calibration plot for $H_2O_2$ determination is linear in the range of 0.5 μM to 2 mM. The sensitivity of PBNPs modified electrode for $H_2O_2$ analysis was found to be 156.5 μA $mM^{-1}$ $cm^{-2}$ with lowest detection limit was 50 nM.

## 1.5 Stability and Reproducibility

The results based on cyclic voltammetry yielded the stability of the electrodes. In this case, peak current and peak potential were found almost unchanged and the amount of degradation after 50 cycles at a scan rate of 10 mV $s^{-1}$ was less than 5% using same batch of electrode material systems. The modified electrode show operational stability for more than 30 days. The relative standard deviation (RSD) of the current response to 1 mM $H_2O_2$ at 0.0 V *vs*. Ag|AgCl is found to be 3.4 for 20 successive measurements.